Sound-Based Imaging: Regularization Approaches in Near-field Acoustic Holography

Thomas Martinod Saldarriaga[a]

This manuscript was compiled on November 12, 2024

Regularization of the inverse problem is a complex issue when using Near-field Acoustic Holography (NAH) techniques to identify vibrating sources. This article aims to compare and implement various regularization methods in the context of NAH. Specifically, it compares the commonly used Tikhonov regularization, sparsity-based regularization and neural networks (NN) regularization for a planar NAH array with measurements obtained from an experimental setup in a previous study [3]. Additionally, it theoretically introduces Green's function-based regularization. The first three types of regularization methods yield images consistent with the results from the referenced study, and statistical indicators are used to determine which method performs best at different frequencies.

Near-field Acoustic Holography | Ill posed problems | Regularization |

1. Introduction

Nearfield Acoustic Holography (NAH) is a technique widely used for measuring the normal velocity scalar field $\dot{w}$ and acoustic pressure field p of vibrating structures based on close-range sound field measurements. This article focuses on the inverse problem of reconstructing the normal velocity distribution $\dot{w}$ of the source structure, which requires regularization due to ill-conditioning [32].

In this study, we also aim to replicate the results presented by Chardon et al. [3] for Tikhonov and sparsity-based regularization techniques. However, instead of using the original software, we will implement these methods using `Python`, providing an accessible approach to solving this inverse problem.

The structure of this article is as follows: Section 2 introduces the continuous and discrete formulations of NAH, focusing on the reconstruction of the normal velocity field at the source $\dot{w}$. In section 3, the importance of regularization is discussed, and several regularization techniques are presented, including Tikhonov, sparsity-based methods, machine learning (via convolutional neural networks), and Green's function. The methodology section details the experimental data used to validate the first three regularization methods and provides a concise overview of the algorithms applied. Finally, the results section assesses the statistical metrics used to evaluate the accuracy of the regularized images against the ground truth, and presents the best regularized images for the experimental data at four different frequencies.

2. Mathematical Formulation of NAH

A. Continuous Formulation. Two primary approaches exist for developing the mathematical framework essential to understanding NAH. The first approach relies solely on the acoustic pressure field [20], [21] while the other is centered on the normal velocity scalar field [3], [13]. The mathematical treatment also heavily relies on the geometry of vibrating structures and the corresponding layout of the sensor array [35]. In this study, only planar geometries are considered.

The pressure p on a plane at elevation z_0, generated by a plate with a normal velocity distribution $\dot{w}(x, y, 0)$ at elevation 0 and frequency ν (or angular frequency $\omega = 2\pi\nu$), is expressed as the convolution of the normal velocity distribution and the propagator $g(\|\vec{r}\|) = g(r) = -i\rho ck e^{ikr}/2\pi r^*$ [33], given by:

*The propagator $g(r)$ in this context represents how sound waves emitted by the vibrating plate "propagate" through space. It accounts for the attenuation and phase shift of the sound waves as they travel from the plate to the observation plane at elevation z_0.

Significance Statement

This article is significant due to its comprehensive exploration and comparison of various regularization methods within the framework of Near-field Acoustic Holography (NAH). It addresses the critical issue of ill-posed inverse problems by evaluating techniques such as Tikhonov regularization, sparsity-based methods, Neural Network regularization, and Green's function-based approaches. By investigating these methods, the study offers valuable insights into how different regularization techniques can enhance the precision and reliability of reconstructing normal velocity distributions in vibrating structures, which is crucial for improving sound-based imaging accuracy. The findings are further strengthened by empirical validation through experimental data, adding robustness to the conclusions.

These advancements hold great importance for industrial applications, including acoustic cameras, pipeline leak detection, and emissions measurement [24], extending the impact of this work beyond sound-based imaging to broader scientific and societal contributions.

Author affiliations: [a]Engineering Physics and Engineering Mathematics at EAFIT University, Medellín, Colombia. tmartinods@eafit.edu.co

$$p(x, y, z_0) = g(x, y, z_0) *_{xy} \dot{w}(w, y, 0). \quad (1)$$

Here, $*_{xy}$ denotes 2-D convolution in the x and y variables, c represents the wave velocity, ρ is the air density, and $k = |\vec{k}| = \omega/c$ denotes the norm of the wavenumber vector. Taking the 2-D spatial transform of Eq. (1) with integration variables x and y results in:

$$P(k_x, k_y, z_0) = G(k_x, k_y, z_0)\dot{W}(k_x, k_y, 0). \quad (2)$$

Here, capital letters indicate the Fourier 2-D transformed variables, and k_x and k_y represent the wavenumbers in the x and y directions, respectively.

B. Discrete Formulation. The standard approach in Nearfield Acoustic Holography involves a discretized representation of Eq. (2), expressed as [30]:

$$\mathbf{p} = \mathbf{F}^{-1}\mathbf{G}\mathbf{F}\dot{\mathbf{w}}. \quad (3)$$

In this formulation:

- $\dot{\mathbf{w}}$ represents the vector of source normal velocities, discretized on a regularly spaced rectangular grid,
- $\mathbf{p}$ denotes the vector of measured pressures, also discretized within the hologram plane,
- $\mathbf{F}$ denotes the 2-D spatial Discrete Fourier Transform (DFT) operator, and
- $\mathbf{G}$ is predominantly zero except on the diagonal, where it is equivalent to G sampled at the wave vectors of the DFT basis vectors [17].

The matrix product $\mathbf{F}^{-1}\mathbf{G}\mathbf{F}$ is denoted as $\mathbf{H}^{\dagger}$, with its conjugate transpose represented as $\mathbf{H}^{\star}$. Solving the inverse problem provides an estimate of the normal velocity $\hat{\dot{w}}$ of the structure. Direct inversion of Eq. (3) yields:

$$\hat{\dot{w}} = \mathbf{F}^{-1}\mathbf{G}^{-1}\mathbf{F}\mathbf{p} = \mathbf{H}^{-1}\mathbf{p}. \quad (4)$$

Since $\mathbf{G}$ is diagonal and easily invertible, naive inversion of this equation is feasible. However, due to its ill-conditioning, the computation of the sources using this approach is highly unstable, necessitating regularization techniques as described in the subsequent section.

3. Regularization Methods

This section elucidates the necessity for regularization and introduces the regularization techniques to be employed.

A. Rationale for Regularization. In the realm of mathematics, a problem is considered well-posed in the Hadamard sense if it satisfies the following criteria:

- The problem possesses a solution.
- The solution is unique.
- Small changes in the initial conditions (data) imply small changes in the response.

[†] The matrix $\mathbf{H}$ in this context can be interpreted as an "operator" that connects the normal velocities of the source with the pressures measured in the plane of the hologram.

Conversely, an ill-posed problem is characterized by the failure of any one of these conditions. In the context of the reconstruction problem posed by NAH, two primary reasons render it ill-posed. Firstly, the fundamental theory of planar NAH needs the hologram to encompass a larger area than the source, ensuring the inclusion of the limits of the acoustic field produced by the vibrating source. Failure to satisfy this criterion results in field truncation, potentially leading to the non-fulfillment of the existence criterion [3].

Secondly, based on wave physics principles, the sensor plane, positioned in close proximity to the source plane, is designed to detect both propagating and evanescent waves. The intensity of evanescent waves diminishes exponentially with distance z. Consequently, during back-propagation calculations, measurement uncertainties can induce significant fluctuations in the source field. Since the back-propagation problem in planar NAH is inherently ill-posed, regularization becomes imperative.

Regularization "transforms" ill-posed problems into well-posed ones by adding constraints or prior information, which stabilizes the solution. This helps prevent overfitting, reduces sensitivity to noise, and ensures that a unique, stable solution can be found, addressing issues like non-uniqueness or instability in the original problem.

B. Tikhonov Regularization. Tikhonov regularization, extensively employed in numerous ill-posed inverse problems, introduces a penalty term to the inverse problem, typically resolving the following minimization problem [9], [11]:

$$\hat{\dot{\mathbf{w}}} = \arg\min_{\dot{\mathbf{w}}} \|\mathbf{p} - \mathbf{H}\dot{\mathbf{w}}\|_2^2 + \lambda\|\mathbf{L}\dot{\mathbf{w}}\|_2^2 . \quad (5)$$

Here, $\mathbf{L}$ represents the Tikhonov matrix, and λ denotes the regularization parameter. The outcome of Tikhonov regularization can be obtained in closed form as:

$$\hat{\dot{\mathbf{w}}} = \mathbf{R}_\lambda \mathbf{H}^{-1}\mathbf{p}, \quad (6)$$

where $\mathbf{R}_\lambda$ is given by:

$$\mathbf{R}_\lambda = \left(\mathbf{H}^{\star}\mathbf{H} + \lambda\mathbf{L}^{\star}\mathbf{L}\right)^{-1}\mathbf{H}^{\star}\mathbf{H}. \quad (7)$$

Two notable points regarding $\mathbf{R}_\lambda$ are:

1. The cancellation of $\mathbf{H}$ and its inverse when Eq. (6) and Eq. (7) are merged circumvents the computation of this ill-conditioned inverse.
2. However, it's worth noting that in the fundamental application of Tikhonov regularization to NAH, where $\mathbf{L}$ is chosen as the identity matrix, $\mathbf{R}_\lambda$ functions acts as low-pass spatial filters[‡] [3].

C. Sparsity Regularization. Sparsity, a fundamental property of signals, refers to their decomposition as a linear combination of a limited number of pre-defined basis functions, termed atoms. Widely utilized across various domains, sparsity finds applications ranging from data compression to source separation and signal analysis.

[‡] In the context of Tikhonov regularization, a low spatial filter smooths the solution by suppressing high-frequency components, effectively reducing noise and preserving important low-frequency information.

Formally, a dictionary $\mathcal{D}$, assumed here to have a finite size M, consists of atoms $\mathbf{d}_k \in \mathbb{R}^N : \mathcal{D} = \{\mathbf{d}_k\}_{k=1\dots M}$. $\mathcal{D}$ can either form a basis of $\mathbb{R}^N$ ($M = N$) or an overcomplete family spanning $\mathbb{R}^N$ ($M > N$).

A discrete signal $\mathbf{x} \in \mathbb{R}^N$ is deemed sparse in $\mathcal{D}$ if it can be represented as a linear combination of a small subset of atoms [3]:

$$\mathbf{x} = \sum_{j \in J} \alpha_j \mathbf{d}_j. \tag{8}$$

where J is a subset of $\{1 \dots M\}$ with $|J| \ll M$. While this decomposition can be exact or approximate, an overcomplete dictionary $\mathcal{D}$ typically lacks a unique representation for a given signal $\mathbf{x}$. To determine the sparsest set of coefficients α satisfying this equation or achieving the best balance between data fidelity and sparsity, numerous algorithms, notably ℓ_1 optimization techniques, have been developed.

In the context of NAH, it is assumed that the discretized version of the Fourier-domain velocity map of the source plane $\hat{w}$ is approximately sparse in a suitable basis:

$$\hat{w} \approx \mathbf{D}\boldsymbol{\alpha}. \tag{9}$$

Here, the vector $\boldsymbol{\alpha}$ comprises only $|J|$ non-zero elements, and $\mathbf{D} \in \mathbb{R}^{n \times m}$ denotes the matrix whose columns represent all the $\mathbf{d}_k$ in $\mathcal{D}$. Consequently, the NAH inverse problem can be reformulated as follows: given a set of pressure measurements $\mathbf{p}$, find the sparsest set of coefficients α_j such that $\mathbf{p} = \mathbf{HD}\boldsymbol{\alpha}$. Mathematically, this problem can be expressed as:

$$\underset{\alpha}{\operatorname{argmin}} \|\boldsymbol{\alpha}\|_1 \text{ subject to } \mathbf{p} = \mathbf{HD}\boldsymbol{\alpha}. \tag{10}$$

It's noteworthy to draw a parallel between Tikhonov regularization Eq. (5) and sparse ℓ_1 regularization. The latter can be represented in Lagrangian form as:

$$\underset{\boldsymbol{\alpha}}{\operatorname{argmin}} \|\mathbf{p} - \mathbf{HD}\boldsymbol{\alpha}\|_2^2 + \lambda \|\boldsymbol{\alpha}\|_1. \tag{11}$$

C.1. Selection of a Dictionary $\mathcal{D}$. Theoretical findings [16] suggest that plane waves offer accurate approximations to solutions of the Helmholtz equation on plates, which are characterized by having a point connectable to any other point via a line segment fully contained within the plate. Notably, all convex plates (as rectangular plates) fall under this category. Recent extensions of these results apply to thin isotropic homogeneous plates.

Mathematically, the plate's velocity $\dot{\mathbf{w}}$, as a solution to the Kirchhoff-Love equation, can be approximated by a combination of plane waves and evanescent waves:

$$\dot{\mathbf{w}}(x, y) \approx \left(\sum_n \alpha_n e^{i\vec{k}_n \cdot \vec{r}} + \beta_n e^{\vec{k}_n \cdot \vec{r}} \right) \mathbf{1}_{\mathcal{S}}(x, y). \tag{12}$$

Here, $\mathbf{1}_{\mathcal{S}}(x, y)$ denotes the indicator function that confines the plane waves to the plate's domain $\mathcal{S}$.

D. Neural Networks Regularization. While this method may seem straightforward compared to others discussed here, it's also the most computationally intensive. Mathematically, both previous regularization methods lead to a non-linear optimization problem (Eq. (5), Eq. (11)). An essential question that arises in such problems is: how to select the penalization parameter λ?

Since this parameter is unbounded above, one can devise a neural network based iterative algorithm aiming to enhance properties desired by the experimenter. In the context of NAH, where the primary objective is detecting sound sources, contrast becomes paramount for proper source detection. This regularization method leverages either Tikhonov regularization or sparsity regularization, followed by the application of a neural network trained to identify images with heightened contrast. Specifically, it seeks to maximize the absolute difference between a pixel and its Cartesian neighbors.

E. Green's Function Regularization. Let us begin by revisiting the Tikhonov regularization optimization problem:

$$\begin{aligned} \hat{\dot{\mathbf{w}}} &= \underset{\dot{\mathbf{w}}}{\operatorname{argmin}}\, E(\dot{\mathbf{w}}) = \underset{\dot{\mathbf{w}}}{\operatorname{argmin}} \|\mathbf{p} - \mathbf{H}\dot{\mathbf{w}}\|_2^2 + \lambda \|\mathbf{L}\dot{\mathbf{w}}\|_2^2 \\ &= \underset{\dot{\mathbf{w}}}{\operatorname{argmin}} \|\mathbf{H}^{-1}\mathbf{p} - \dot{\mathbf{w}}\|_2^2 + \lambda \|\mathbf{L}\dot{\mathbf{w}}\|_2^2 . \end{aligned} \tag{13}$$

where $\mathbf{L}$ is the Tikhonov matrix, λ is the regularization parameter, and E is the Tikhonov functional. The concept behind this regularization method is to minimize the functional E by applying the first-order optimality condition $\delta E = 0$ to derive the Euler-Lagrange equations in $\mathbb{R}^3$. The final result derived from this process is [22]:

$$\hat{\dot{\mathbf{w}}}_k(\vec{r}) = \frac{1}{\lambda} \sum_{j=1}^{N} [(\mathbf{H}^{-1}\mathbf{p})_j - \hat{\dot{\mathbf{w}}}(\vec{r}_j)]\, G(\vec{r}_k - \vec{r}_j), \tag{14}$$

which signifies that each component of the normal velocities can be expanded in terms of the columns of the Green's matrix $[G(\vec{r}_k - \vec{r}_j)]_{kj}$. However, the computational implementation of this method proved to be impractical, as it requires prior knowledge of the form of the Green's functions, or iteratively approximating their coefficients in a basis to achieve effective regularization.

4. Methodology

As previously mentioned, this paper focuses purely on mathematical and computational aspects, without conducting any experimental setup. To evaluate the different regularization methods discussed earlier, a reference study with credible and reproducible results is necessary for testing against the proposed methods. The selected reference for conducting the experiments is the article by Chardon and Daudet titled *Nearfield Acoustic Holography using sparsity and compressive sampling principles* [3]. In this study, the authors conducted a physical experiment on a guitar, measuring the discrete acoustic pressure field $\mathbf{p}$ at four different frequencies ($\nu = 78$Hz, 402Hz, 1483Hz, and 3297Hz) to recover the normal velocity field $\dot{w}$. The obtained results were compared with reference (ground truth) measurements

of the same experiment.

The ground truth measurements were acquired using a laser vibrometer to measure the actual velocity field of the source on a fine regular grid, providing $50 \times 40 = 2000$ vibration impulse responses. For the rectangular plate mentioned, the grid had a 10 mm step size along both coordinate axes. The acoustic impulse responses measured by the microphones were processed to provide holograms in the temporal Fourier domain. These holograms, representing harmonic pressure fields, were used for the NAH method. Hologram measurements were performed with an array of 120 electret microphones and a custom-built 128-channel digital recorder. The standard NAH hologram was collected using a 12×10 regular microphone array with a 50 mm square step. The overall dimensions of the array were 550 mm x 450 mm. The array was placed at a distance of $z_0 = 20$ mm from the rectangular plate.

With the data source (the matrix $\mathbf{p}$) identified, the computational analysis conducted in this research is presented step by step:

a) The open-source code (in `MATLAB`) provided by the authors in [3] was accessed and executed, verifying that the results of the code aligned with those reported in the article. Also, databases provided in the same article containing the matrix $\mathbf{p}$ were retreived.

b) For Tikhonov regularization, both the matrix Eq. (6) and an optimization solver integrated into the `scipy.optimize` library were employed to solve the nonlinear problem Eq. (5), verifying that they yielded nearly identical results for $\dot{\mathbf{w}}$.

c) For sparsity regularization, the matrix $\mathbf{p}$ was initially expanded into the basis given by Eq. (12) (via direct inner product), ensuring that the majority of coefficients (up to $n = 20$) were zero. Subsequently, the expression Eq. (9) was directly employed to compute the normal velocities in the source plane instead of solving the associated optimization problem.

d) For NN regularization, the nonlinear optimization problem Eq. (11) was solved to prioritize images with higher contrast by selecting λ. To achieve this, a neural network was trained using `pytorch` based on the results obtained in [3].

e) Finally, the magnitude images of the normal velocity field were stored in `.csv` files and plotted using the `matplotlib` library after calculating the statistical indicators that will be presented in the next section.

5. Results

This section presents the statistical indicators used to discern which regularization method produced an image most similar to the ground truth, followed by the images with best indicators.

A. Statistical Indicators. Four basic statistical indicators were employed for image similarity analysis. Simbolcally: C, ε_1, ε_2, and M.

The coefficient of correlation C measures the degree of linear relationship between two images' pixel values. It ranges from -1 to 1, where 1 indicates a perfect positive correlation, and 0 suggests little to no correlation. The correlation coefficient was calculated using the `correlate2d` method from the `scipy.signal` library.

The first-order Root Mean Square Error (RMSE) ε_1 quantifies the average difference between corresponding pixel values of two images. It provides a measure of the overall discrepancy or deviation between the images, with a value of 0 indicating equality. The second-order RMSE ε_2 measures the same but compares the ground truth and the regularized image after applying a first-order blur[§].

The mean absolute error M is the only dimensional indicator, representing error in units of m/s. While all indicators are crucial and measure the performance of the regularized images, a hierarchical preference is used to select the better image, following the order presented. For the first frequency, $\nu = 78$ Hz, the ground truth image is shown in Fig. 1.

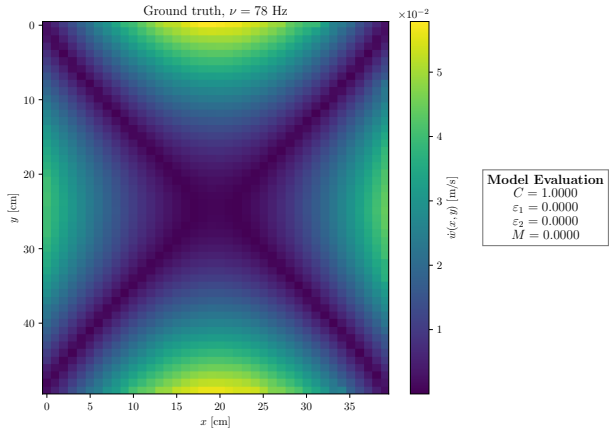

Fig. 1. Ground truth image at $\nu = 78$ Hz.

Among the three regularized images, the one using NN and sparsity regularization yielded the most favorable results. Shown in Fig. 2, this method succeeded in identifying sound sources, with a correlation of $C = 0.92$ with the ground truth.

For the mid-range frequency $\nu = 402$ Hz, the closest regularized image to the ground truth was obtained using Tikhonov regularization, with a correlation of $C = 0.94$, as shown in Fig. 3.

The results for the frequency $\nu = 1483$ Hz are not presented here. Readers are encouraged to refer to the Appendices and Reproducible Research section, where they can find the images for the methods that were not the closest to the ground truth, along with the ground truth

[§]A first-order blur with a 3×3 kernel averages the pixel values by applying a simple filter where each pixel is replaced by the average of itself and its 8 surrounding neighbors. The 3×3 kernel typically contains equal weights, and the convolution operation smooths the image, reducing sharp edges and noise.

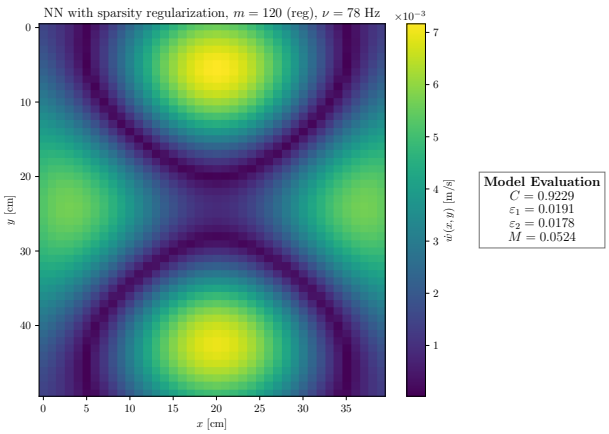

Fig. 2. NN and sparsity regularized image at $\nu = 78$ Hz.

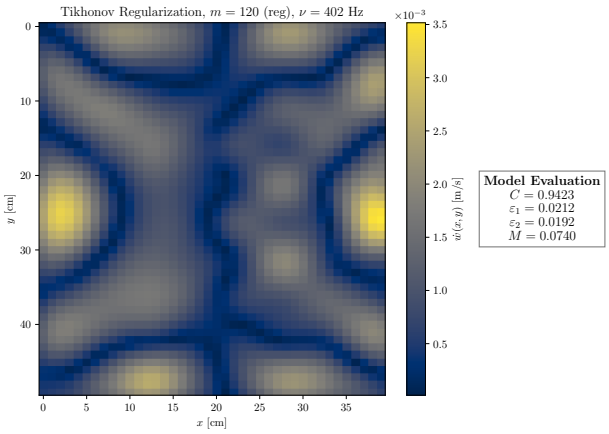

Fig. 3. Tikhonov regularized image at $\nu = 402$ Hz.

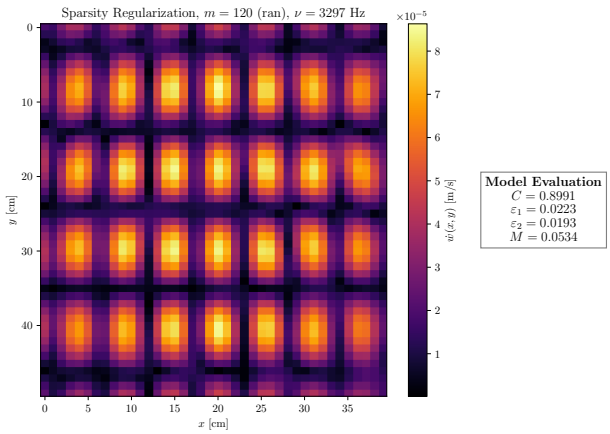

Fig. 4. NN and sparsity regularized image at $\nu = 3297$ Hz.

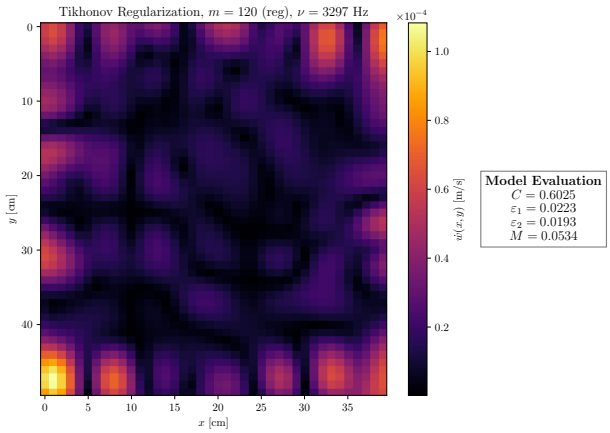

Fig. 5. Tikhonov regularized image at $\nu = 3297$ Hz.

images for each frequency. For this frequency, the closest regularization method was sparsity without NN, suggesting that the original image lacked extreme contrasts, and refining λ based on this criterion induced errors.

Similarly, at the high frequency $\nu = 3297$ Hz, both sparsity without NN and NN regularization methods effectively reproduced the ground truth image. Fig. 4 displays the best regularized image, while Tikhonov regularization, as depicted in Fig. 5, catastrophically failed due to acting as a lowpass frequency filter in the wavenumber space at higher frequencies [3], [27].

6. Conclusions

The primary objective of this paper was to evaluate and compare different regularization methods in the context of planar NAH. Also, the article presented satisfied the goal of formally describing NAH and the regularization methods used for creating the images shown, also exhibiting their computational implementation. On the other hand, comparisons between the methods were based on strong statistical evidence, and even though no much comment was made on indicators other than C is left to the readers choice his/her preference on which indicator to consider.

The main advance this article represents is that it is one of the first approaches to regularization methods in NAH at a national level.

Finally, as a brief comment on the results section, the order of magnitude of the normal velocity field does not represent any specific physical property. Instead, the contrast (i.e., the differences in normal velocities) is used to identify the locations of the sources. As shown, this objective was successfully achieved.

7. Appendices and reproducible research

All contents, codes, appendices and data used throught this investigation are located at the repository https://github.com/thomas-martinod/proyecto-avanzado-1 under the MIT licence (the contents are mainly in spanish), in alignment with the reproducible research and open science principles [15], [14], [12].

ACKNOWLEDGMENTS. This project would not have been possible without the constant support and technical guidance of my tutor, Professor Nicolás Guarín Zapata from the School of Applied Sciences and Engineering at Universidad EAFIT. Additionally, special thanks to Professor Elena Montilla Rosero from the same institution for her valuable mentorship. Finally, I extend my heartfelt gratitude to my family, Jules, JuanFer, Fer, and Yoshiro, for their unwavering support.

References

[1] Eugenia Anello. *A Comprehensive Guide of Regularization Techniques in Deep Learning*. Understanding how Regularization can be useful to improve the performance of your model. Dec. 28, 2021. URL: https://towardsdatascience.com/a-comprehensive-guide-of-regularization-techniques-in-deep-learning-c671bb1b2c67 (visited on 02/15/2024).

[2] George Bissinger, Earl G. Williams, and Nicolas Valdivia. "Violin f-hole contribution to far-field radiation via patch near-field acoustical holography". In: *The Journal of the Acoustical Society of America* 121.6 (June 1, 2007), pp. 3899–3906. ISSN: 0001-4966, 1520-8524. DOI: 10.1121/1.2722238. URL: https://pubs.aip.org/jasa/article/121/6/3899/537263/Violin-f-hole-contribution-to-far-field-radiation (visited on 02/14/2024).

[3] Gilles Chardon et al. "Near-field acoustic holography using sparse regularization and compressive sampling principles". In: *The Journal of the Acoustical Society of America* 132.3 (Sept. 1, 2012), pp. 1521–1534. ISSN: 0001-4966, 1520-8524. DOI: 10.1121/1.4740476. URL: https://pubs.aip.org/jasa/article/132/3/1521/936549/Near-field-acoustic-holography-using-sparse (visited on 02/14/2024).

[4] Tatsuki Fushimi, Kenta Yamamoto, and Yoichi Ochiai. "Acoustic hologram optimisation using automatic differentiation". In: *Scientific Reports* 11.1 (June 16, 2021). Code repository: https://zenodo.org/records/4906351, p. 12678. ISSN: 2045-2322. DOI: 10.1038/s41598-021-91880-2. URL: https://www.nature.com/articles/s41598-021-91880-2 (visited on 03/02/2024).

[5] Tatsuki Fushimi, Kenta Yamamoto, and Yoichi Ochiai. "Acoustic hologram optimisation using automatic differentiation". In: *Scientific Reports* 11.1 (June 16, 2021), p. 12678. ISSN: 2045-2322. DOI: 10.1038/s41598-021-91880-2. URL: https://www.nature.com/articles/s41598-021-91880-2 (visited on 03/14/2024).

[6] Parameswaran Hariharan. *Basics of holography*. Cambridge, UK New York, NY: Cambridge University Press, 2002. 161 pp. ISBN: 978-0-521-00200-4 978-0-521-80741-8.

[7] Sabih I. Hayek. "Nearfield Acoustical Holography". In: *Handbook of Signal Processing in Acoustics*. Ed. by David Havelock, Sonoko Kuwano, and Michael Vorländer. New York, NY: Springer New York, 2008, pp. 1129–1139. ISBN: 978-0-387-77698-9 978-0-387-30441-0. DOI: 10.1007/978-0-387-30441-0_59. URL: http://link.springer.com/10.1007/978-0-387-30441-0_59 (visited on 02/14/2024).

[8] Bernard P. Hildebrand and Byron B. Brenden. *An introduction to acoustical holography*. A Plenum/Rosetta edition. New York: Plenum Publ. Co, 1974. 224 pp. ISBN: 978-0-306-20005-2.

[9] María Josefina Carrió. "Regularización de problemas inversos mal condicionados mediante la minimización de funcionales de tipo Tikhonov-Phillips doblemente generalizados". MSc. Colombia: Universidad Nacional del Litoral, 2019. 100 pp. URL: https://bibliotecavirtual.unl.edu.ar:8443/bitstream/handle/11185/5466/Tesis.pdf?sequence=1&isAllowed=y (visited on 02/15/2024).

[10] Yang-Hann Kim. "Acoustic Holography". In: *Springer Handbook of Acoustics*. Ed. by Thomas D. Rossing. New York, NY: Springer New York, 2014, pp. 1115–1137. ISBN: 978-1-4939-0754-0 978-1-4939-0755-7. DOI: 10.1007/978-1-4939-0755-7_26. URL: http://link.springer.com/10.1007/978-1-4939-0755-7_26 (visited on 02/15/2024).

[11] Nguyen Van Kinh. "On the Regularization Method for Solving Ill-Posed Problems with Unbounded Operators". In: *Open Journal of Optimization* 11.2 (2022), pp. 7–14. ISSN: 2325-7105, 2325-7091. DOI: 10.4236/ojop.2022.112002. URL: https://www.scirp.org/journal/doi.aspx?doi=10.4236/ojop.2022.112002 (visited on 02/14/2024).

[12] Christopher Steven Marcum and Ryan Donohue. *Breakthroughs for All: Delivering Equitable Access to America's Research*. OSTP blog. Aug. 25, 2022. URL: https://www.whitehouse.gov/ostp/news-updates/2022/08/25/breakthroughs-for-alldelivering-equitable-access-to-americas-research/ (visited on 02/15/2024).

[13] J. D. Maynard, E. G. Williams, and Y. Lee. "Nearfield acoustic holography: I. Theory of generalized holography and the development of NAH". In: *The Journal of the Acoustical Society of America* 78.4 (Oct. 1, 1985), pp. 1395–1413. ISSN: 0001-4966, 1520-8524. DOI: 10.1121/1.392911. URL: https://pubs.aip.org/jasa/article/78/4/1395/779266/Nearfield-acoustic-holography-I-Theory-of (visited on 02/14/2024).

[14] MINISTERIO DE CIENCIA TECNOLOGÍA E INNOVACIÓN – MINCIENCIAS. *Política Nacional de Ciencia Abierta*. May 27, 2022. URL: https://minciencias.gov.co/sites/default/files/ckeditor_files/Documento%20consulta%20p%C3%BAblica%20-%20Pol%C3%ADtica%20Nacional%20de%20Ciencia%20Abierta.pdf (visited on 02/15/2024).

[15] MINISTERIO DE CIENCIA, TECNOLOGÍA E INNOVACIÓN. *Política Pública de Apropiación Social del Conocimiento en el marco de la CTeI*. Mar. 2021. URL: https://minciencias.gov.co/sites/default/files/politica_publica_de_apropiacion_social_del_conocimiento.pdf (visited on 02/15/2024).

[16] A. Moiola, R. Hiptmair, and I. Perugia. "Plane wave approximation of homogeneous Helmholtz solutions". In: *Zeitschrift für angewandte Mathematik und Physik* 62.5 (Oct. 2011), pp. 809–837. ISSN: 0044-2275, 1420-9039. DOI: 10.1007/s00033-011-0147-y. URL: http://link.springer.com/10.1007/s00033-011-0147-y (visited on 05/29/2024).

[17] R. K. Mueller and N. K. Sheridon. "Sound Holograms and Optical Reconstruction". In: *Applied Physics Letters* 9.9 (Nov. 1, 1966), pp. 328–329. ISSN: 0003-6951. DOI: 10.1063/1.1754771. URL: https://doi.org/10.1063/1.1754771 (visited on 03/10/2024).

[18] Jia-cheng Ni et al. "L1/2 Regularization Sar Imaging Via Complex Image Data: Regularization Parameter Selection for Target Detection Task". In: *IGARSS 2018 - 2018 IEEE International Geoscience and Remote Sensing Symposium*. IGARSS 2018 - 2018 IEEE International Geoscience and Remote Sensing Symposium. Valencia: IEEE, July 2018, pp. 2298–2301. ISBN: 978-1-5386-7150-4. DOI: 10.1109/IGARSS.2018.8519138. URL: https://ieeexplore.ieee.org/document/8519138/ (visited on 02/14/2024).

[19] Luis Rincón. *Curso Intermedio de Probabilidad*. Ciudad de México: Facultad de Ciencias UNAM, Oct. 2007. URL: http://personal.cimat.mx:8181/~pabreu/LuisRincon.pdf.

[20] R. (Rick) Scholte. "Fourier based high-resolution near-field sound imaging". In: (2008). In collab. with Roozen NB (Bert), Nijmeijer H (Henk), and Lopez I (Ines). Publisher: [object Object]. DOI: 10.6100/IR639528. URL: https://research.tue.nl/en/publications/fourier-based-highresolution-nearfield-sound-imaging(1bd464b0-e91c-4573-bb81-6a72fa0c289d).html (visited on 03/14/2024).

[21] Rick Scholte. *Fourier Based Near Field Acoustic Holography*. Eindhoven University of Technology, Mar. 31, 2015. URL: https://www.youtube.com/watch?v=AEJSE_GKozE&ab_channel=Sorama.

[22] S Sengupta. *Lec-27 Solution of Regularization Equation: Greens Function*. URL: https://www.youtube.com/watch?v=4U3P0LcaJcw&ab_channel=nptelhrd (visited on 05/29/2021).

[23] Howard M. Smith. *Principles of holography*. New York: Wiley-Interscience, 1969. 239 pp. ISBN: 978-0-471-08340-5.

[24] Sorama. *Sorama - Make sound insightful*. https://sorama.eu/.

[25] Steve Mould. *Acoustic cameras can SEE sound*. Mar. 20, 2023. URL: https://www.youtube.com/watch?v=QtMTvsi-4Hw (visited on 03/02/2024).

[26] Albert Tarantola. *Inverse Problem Theory and Methods for Model Parameter Estimation*. Society for Industrial and Applied Mathematics, Jan. 2005. ISBN: 978-0-89871-572-9 978-0-89871-792-1. DOI: 10.1137/1.9780898717921. URL: http://epubs.siam.org/doi/book/10.1137/1.9780898717921 (visited on 02/15/2024).

[27] A. N. Tikhonov and V. IA Arsenin. *Solutions of ill-posed problems*. Scripta series in mathematics. Washington : New York: Winston ; distributed solely by Halsted Press, 1977. 258 pp. ISBN: 978-0-470-99124-4.

[28] Nicolas P. Valdivia. "Krylov Subspace iterative methods for time domain boundary element method based nearfield acoustical holography". In: *Journal of Sound and Vibration* 484 (Oct. 2020), p. 115498. ISSN: 0022460X. DOI: 10.1016/j.jsv.2020.115498. URL: https://linkinghub.elsevier.com/retrieve/pii/S0022460X20303308 (visited on 02/15/2024).

[29] David Lee Van Rooy. "Digital Ultrasonic Wavefront Reconstruction in the Near Field". Texto. Rice University, 1971. 81 pp. URL: https://repository.rice.edu/items/dbeb39f7-30af-4df1-8ffb-67c148615054 (visited on 02/13/2024).

[30] W. A. Veronesi and J. D. Maynard. "Nearfield acoustic holography (NAH) II. Holographic reconstruction algorithms and computer implementation". In: *The Journal of the Acoustical Society of America* 81.5 (May 1, 1987), pp. 1307–1322. ISSN: 0001-4966. DOI: 10.1121/1.394536. URL: https://doi.org/10.1121/1.394536 (visited on 03/10/2024).

[31] Wikipedia. *Holography*. URL: https://en.wikipedia.org/wiki/Holography.

[32] Earl G. Williams, J. D. Maynard, and Eugen Skudrzyk. "Sound source reconstructions using a microphone array". In: *The Journal of the Acoustical Society of America* 68.1 (July 1, 1980), pp. 340–344. ISSN: 0001-4966, 1520-8524. DOI: 10.1121/1.384602. URL: https://pubs.aip.org/jasa/article/68/1/340/773621/Sound-source-reconstructions-using-a-microphone (visited on 02/14/2024).

[33] Earl George Williams. *Fourier acoustics: sound radiation and nearfield acoustical holography*. San Diego, Calif: Academic Press, 1999. ISBN: 978-0-12-753960-7.

[34] Qing Wu, Tianlu Ma, and Fan Wang. "Modified Lanczos Algorithm for L2,1 norm Regularization Extreme Learning Machine". In: *2021 International Conference on Control, Automation and Information Sciences (ICCAIS)*. 2021 International Conference on Control, Automation and Information Sciences (ICCAIS). Xi'an, China: IEEE, Oct. 14, 2021, pp. 679–684. ISBN: 978-1-66544-029-5. DOI: 10.1109/ICCAIS52680.2021.9624517. URL: https://ieeexplore.ieee.org/document/9624517/ (visited on 02/15/2024).

[35] Xuxin Zhang et al. "Statistically Optimized Near-Field Acoustic Holography Using Prolate Spheroidal Wave Functions". In: *Shock and Vibration* 2023 (Aug. 31, 2023). Ed. by Arcanjo Lenzi, pp. 1–20. ISSN: 1875-9203, 1070-9622. DOI: 10.1155/2023/9954054. URL: https://www.hindawi.com/journals/sv/2023/9954054/ (visited on 02/15/2024).